Chapter 5

N-Type Doped μc-Si:H

In section 4 results of intrinsic films of μc-Si:H with a systematic variation of material structure ranging from highly crystalline to amorphous growth were shown. ESR measurements have been used to determine the spin density N_S. However, from these investigations it is not clear how far N_S correlates with the defect density in the material and if the spin density N_S is a measure of the real defect density N_{DB}. This is the subject of the following section.

For this purpose, material prepared with different SC=[SiH_4]/([H_2]+[SiH_4]) and phosphorous doping levels PC =[PH_3]/([PH_3]+[SiH_4]) will be studied. The silane concentration was varied in the range from SC = 2% to 8%, resulting in structure compositions comparable to those studied in Chapter 4. The doping concentrations PC of 1, 5, and 10 ppm were chosen to be of the order of the intrinsic spin density N_S (see Fig. 4.5 (a)). To study effects of doping on the position of the Fermi level and the occupation of defect states, electrical dark conductivity σ_D and ESR measurements have been performed.

5.1 Structure Characterization

In order to obtain a measure of the crystalline volume content, Raman spectra were recorded on both glass and aluminum substrates. The results are summarized in Fig. 5.1 (a), showing the Raman intensity ratio I_C^{RS} plotted versus the silane concentration SC. For doping concentrations in the range of $1-10$ ppm the transition from highly crystalline to predominantly amorphous growth can be observed. In the highly crystalline growth regime between SC=2% and 5%, the Raman intensity ratio decreases only slightly from I_C^{RS}=0.85 to 0.74 and the spectra are dominated by the crystalline signal. Above SC=5% the transition to amorphous growth can be observed. An increasing amorphous phase contribution results in a fairly steep decrease of I_C^{RS} between SC=5% and 7%. For silane concentra-

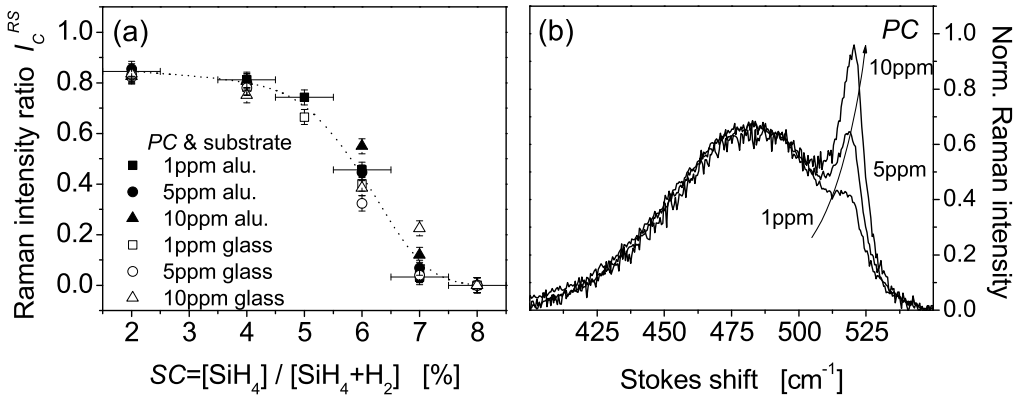

Figure 5.1: *(a) Raman intensity ratio (I_C^{RS}) for samples deposited on aluminum (closed symbols) and glass (open symbols). (b) Raman spectra of μc-Si:H prepared at SC = 7% with varying doping concentrations of PC =1, 5, and 10 ppm). With increasing doping concentration the crystallinity increases.*

tions higher than SC=7% the Raman spectra show only the amorphous peak at 480 cm^{-1}. Comparing samples deposited on glass and aluminum, the well known substrate dependence on the material structure can be observed (compare with Fig. 4.1). Samples deposited on glass in general show a higher amorphous phase contribution and therefore a smaller value of I_C^{RS} compared to material deposited on aluminum.

This has to be kept in mind as in the following section results from conductivity measurements as well as ESR measurements will be compared, where glass and aluminum substrates were used, respectively. Also with increasing doping concentration PC the Raman intensity ratio increases. This is shown in Fig. 5.1 (b), where for a given silane concentration SC the crystallinity increases with increasing doping concentration.

5.2 Electrical Conductivity

Conductivity measurements, as described in section 3.1.3, were performed on films deposited on glass substrates. The results are shown in Fig. 5.2 (a), where the dark conductivities σ_D of phosphorous doped material with PC = 1, 5, and 10 ppm are plotted together with conductivity data of undoped material taken from reference [18]. For the undoped material the conductivity σ_D decreases only slightly between I_C^{RS} =0.82 and 0.47. As a consequence of the structural transition, for material with an I_C^{RS} lower than 0.4 σ_D decreases by several orders of magnitude, resulting in values below 10^{-10} S/cm typical for a-Si:H [65]. Doping effects can

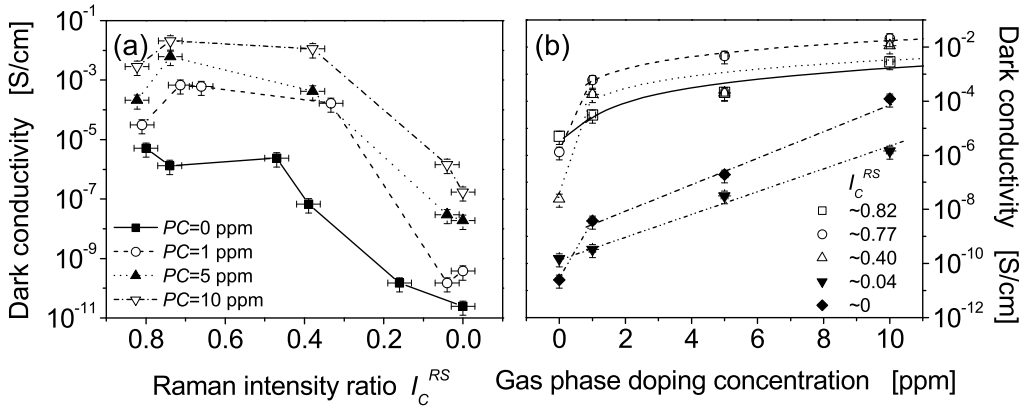

Figure 5.2: *Room temperature conductivity σ_D of μc-Si:H films with doping concentrations of 0 ppm (■), 1 ppm (○), 5 ppm (▲) and 10 ppm (▽) as a function of (a) Raman intensity ratio (I_C^{RS}) and (b) gas phase doping concentration. The data of the undoped material were taken from reference [18].*

be observed for all structure compositions from highly crystalline to amorphous. However, unlike the undoped material for the n-type doped samples the highest σ_D values are not found for the samples with the highest crystallinity. In fact, for all doping concentrations $PC = 1 - 10$ ppm an increase of σ_D by more than one order of magnitude can be observed if the crystallinity decreases from $I_C^{RS} = 0.82$ to 0.77. This indicates that the doping induced free charge carrier concentration is considerably less for the highly crystalline material. Between $I_C^{RS} = 0.77$ and 0.4 σ_D stays almost constant before it drops down by about 5 orders of magnitude as result of the structural transition to predominantly amorphous growth, independent of the particular doping concentration.

In Fig. 5.2 (b) the conductivity is plotted versus the gas phase doping concentration PC. In these plots the correlation between doping and conductivity becomes more obvious. Within the microcrystalline growth regime between $I_C^{RS} \sim 0.82 - 0.40$ (upper three curves in the figure) the doping induced changes of σ_D are highest for samples with $I_C^{RS} \sim 0.77$ and 0.4 and considerably less for the sample with the highest crystallinity. Applying a doping concentration of $PC = 1$ ppm, the dark conductivity of the $I_C^{RS} = 0.77$ and $I_C^{RS} = 0.4$ material changes by more than three orders of magnitude, compared to the undoped material. On the other hand, for the highest crystallinity, where the highest N_S is observed in the undoped material, σ_D increases by only a factor of 6. Plotting σ_D on a linear scale, one observes that for doping concentrations higher than $PC = 1$ ppm all microcrystalline samples ($I_C^{RS} = 0.82 - 0.4$) show an almost linear increase of the conductivity with a structure independent slope. For amorphous or almost

amorphous samples (I_C^{RS} = 0.04 to 0) the dark conductivity shows much lower values over the whole doping range investigated. However, for the I_C^{RS} = 0.04 material σ_D increases exponentially by about 4 orders of magnitude, while for the fully amorphous material σ_D changes by almost 7 orders of magnitude from $\sigma_D = 2\times10^{-11}$ S/cm to 1×10^{-4} S/cm.

The dark conductivity follows nicely the expected behavior. Considering the characteristic of the spin density of the undoped material (see Fig. 4.5 (a)), the results are in agreement with the proposed doping mechanism of compensation of gap states as described in section 2.2.2. Doping induced changes are highest for material for which low spin densities are found in the undoped state. For highly crystalline material, which also exhibits the highest spin densities, the doping induced changes are considerably less, as more defect states have to be compensated before the Fermi level moves up into the conduction band-tail.

5.3 ESR Spectra

Samples prepared for ESR measurements have been deposited on aluminum substrates in the same run as that used for conductivity measurements. The material was then powdered using the procedure described in section 3.3.1. ESR measurements were performed at a temperature of T = 40K. All spectra were normalized to the same peak height and plotted in Fig. 5.3. Fig. 5.3 shows stack plots of samples with different crystallinity ranging from $I_C^{RS} = 0.82 - 0$ and doping concentrations of 1, 5, 10 ppm. The fact that the Raman intensity ratio for the predominantly amorphous material I_C^{RS} = 0.08 deviates slightly from that found in Fig. 5.2 (I_C^{RS} = 0.04) is a direct result of the substrate dependence. The vertical dotted lines in Fig. 5.3 indicate the resonances at g=2.0043, g=2.0052, and g=1.996-1.998, typically found in μc-Si:H (see section 2.2.2).

All spectra show contributions of the three well-known signals at g-values of 2.0043 (db_1), 2.0052 (db_2), and g=1.996-1.998 (CE) (for details see section 2.2.2), except for the spectra taken from the purely amorphous material (I_C^{RS} = 0). Quite surprisingly, the CE resonance can be observed in all spectra of the doped samples, in the highly crystalline material as well as in material where very little Raman intensity due to the crystalline phase is found ($I_C^{RS} < 10\%$). Only samples with no detectable contribution from the crystalline volume to the Raman signal show only the dangling bond signal at g=2.0052. For a given doping level, the intensity of the CE-line is highest for highly crystalline material with an I_C^{RS} of 0.77 or 0.47. The CE line is much less pronounced for the highest crystallinity (I_C^{RS} = 0.82), which is in agreement with the high spin densities found in this material (see Fig. 4.5 (a)). As expected, the intensity of the CE resonance increases

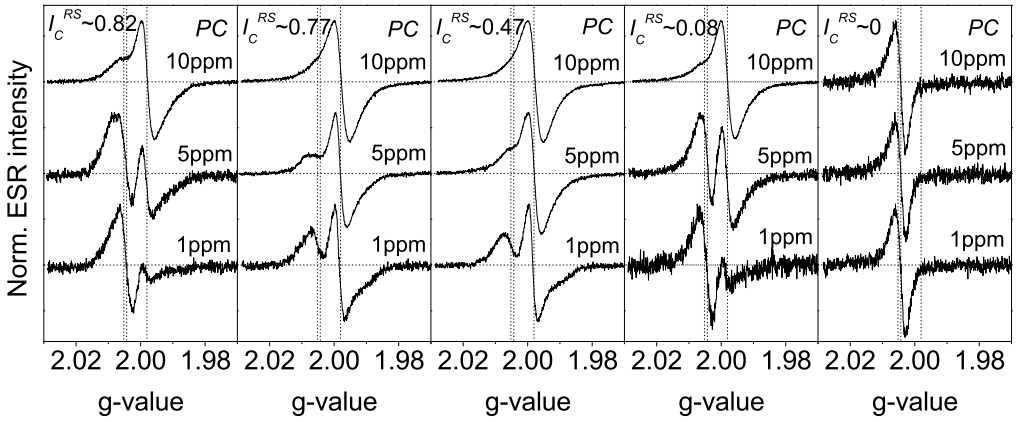

Figure 5.3: *ESR spectra of samples with crystallinities of I_C^{RS} ≈0.82, 0.72, 0.47, 0.08, and 0 with gas phase doping concentrations of PC =1, 5, and 10 ppm measured at T=40K. The vertical dotted lines indicate the position of db_1, db_2, and CE resonances at values of g=2.0043, g=2.0052, and g=1.996-1.998, respectively, typically found in μc-Si:H.*

with increasing doping level *PC*. In addition to the CE signal, the DB signal (db_1+db_2) is visible in all samples, although in the case in which the CE line is most dominating (e.g. $I_C^{RS} = 0.77$ and with $PC = 10$ ppm) the DB signal is at the lower limit for a multi-peak de-convolution analysis to be feasible.

Doping induced effects can be observed in all spectra of material where a crystalline phase can be observed ($I_C^{RS} > 0$). The existence of the resonance at g=1.996-1.998 is a direct result of a shift of E_F up into the conduction band- tail. With increasing doping concentration, more and more states in the conduction band-tail are getting occupied and contribute to the intensity of the resonance. The shift of the Fermi level, however, is governed by the compensation of gap states. For a fixed doping concentration, the high defect density in the $I_C^{RS} \approx 0.82$ material leads to a considerable lower CE spin density N_{CE} compared to the low defect material $I_C^{RS} \approx 0.77$ and 0.47. It is quite surprising, that even for material with crystalline grains that are highly diluted in an amorphous phase ($I_C^{RS} \approx 0.08$) a strong CE line can be observed.

5.4 Dangling Bond Density

To obtain the spin density of each superimposed line shown in Fig. 5.3, a numerical fitting procedure was applied. The DB-signals at g=2.0043 and g=2.0052 could be well approximated by Gaussian lines. For the CE line at g=1.996−1.998 a convolution of a Gaussian and Lorentzian curve was used. However, a separa-

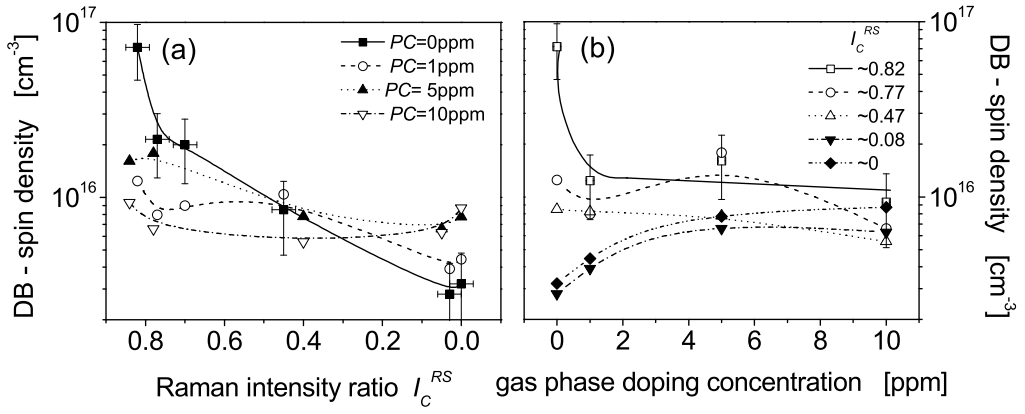

Figure 5.4: *Dangling bond spin density versus I_C^{RS} obtained from numerical fitting of the ESR line shown in Fig. 5.3 (a) vs. the Raman intensity ratio I_C^{RS} and (b) vs. the gas phase doping concentration PC .*

tion of the two DB signals is impossible from the spectra shown above; therefore only the sum of both will be analyzed in this section.

Fig. 5.4 (a) shows the dangling bond (DB) density obtained from this deconvolution procedure versus the Raman intensity ratio I_C^{RS}. Additionally, the DB density N_{DB} for the undoped material is shown. As already shown in Chapter 4 for the intrinsic material, the DB density N_{DB} decreases with increasing amorphous phase contribution. In principle one can observe the decrease of N_{DB} upon decreasing I_C^{RS} for all doping concentrations, but with increasing doping level this phenomena is less pronounced. It is surprising indeed that even for the highest doping concentrations of PC = 10 ppm, DB states can still be observed in all samples. However, depending on the crystallinity there are some distinct differences in how the dangling bond density N_{DB} changes as a function of PC. This is shown in Fig. 5.4 (b), where the spin density is plotted versus the gas phase doping concentration. For the highly crystalline sample (I_C^{RS} = 0.82) the spin density decreases steeply from 0 ppm to 1 ppm and stays almost constant at $N_{DB} \approx 10^{16}$ cm^{-3} for higher doping concentrations. For the highly crystalline samples (I_C^{RS} = 0.77−0.47) the spin density stays almost constant or slightly decreases from already low values of $N_{DB} = 1\times10^{16}$ cm^{-3} for PC=0 ppm to $N_{DB} = 6\times10^{15}$ cm^{-3} for PC=10 ppm. This is a result of compensation. For samples with an even higher amorphous phase contribution ($I_C^{RS} < 0.10$), an increasing dangling bond density can be observed. It seems unlikely that the reason for the increasing N_{DB} is caused by the doping induced dangling bond creation, known from hydrogenated amorphous silicon [89, 90], because these states can not be observed in ESR. It is more plausible that within the investigated doping range, the occupation

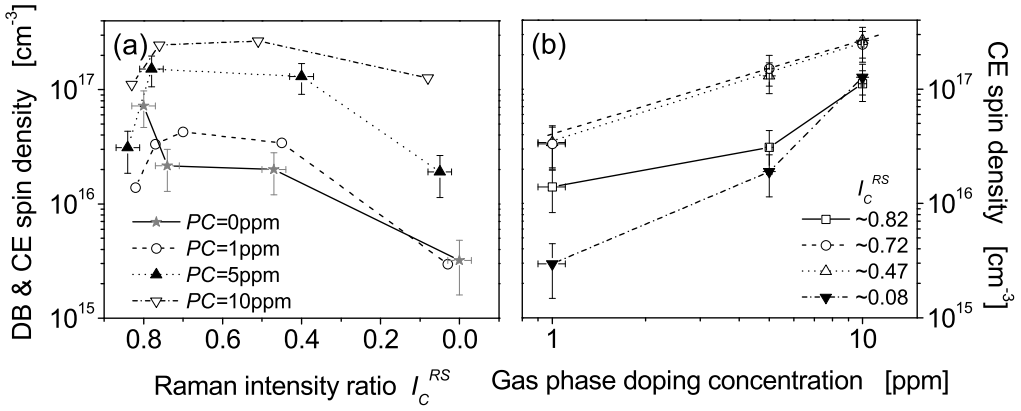

Figure 5.5: *(a) Spin density of the CE resonance (N_{CE}) in the doped samples and the DB resonance (N_{CE}) in undoped material; (b) CE intensity of the microcrystalline phase as a function of conductivity.*

of D^+ states by an electron creating an D^0 state exceeds the compensation of D^0 states. This would be the case if in the undoped state the mean energy position of the defect is above E_F. Material prepared at yet higher doping concentration could give additional proof for this thesis.

The dangling bond signal can be detected in all spectra for all gas phase doping concentrations investigated. Within the highly crystalline regime, N_{DB} decreases between PC = 0 ppm and 1 ppm, but stays almost constant for higher doping concentrations.

5.5 Conduction Band-Tail States

The deconvolution into the individual lines can also be used to determine the number of paramagnetic states in the conduction band-tail. The results for the calculated CE spin density N_{CE} for different doping levels are shown in Fig. 5.5 (a) as a function of I_C^{RS}. Additionally, the dangling bond densities N_{DB} for undoped material are plotted in the graph. The variation of N_{CE} as a function of I_C^{RS} and PC follows nicely the same qualitative behavior as the conductivity plotted in Fig. 5.2 (a). This confirms earlier studies on n-doped highly crystalline material [35, 39]. As expected, the intensity of the CE signal seems to be moderated by the dangling bond density. Material exhibiting the highest crystallinity $I_C^{RS} = 0.82$ and also the highest N_{DB} shows lower CE line intensity compared to the $I_C^{RS} = 0.72$ and $I_C^{RS} = 0.47$ material, where lower N_{DB} are observed. For samples with a crystalline volume fraction lower than $I_C^{RS} = 0.47$ the influence of N_{DB} on doping is masked by effects of the structural change. ESR as an integrating measurement

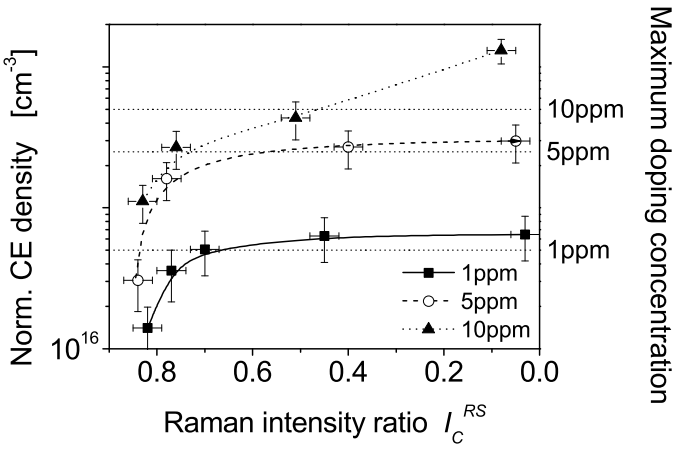

Figure 5.6: *Normalized CE spin densities $N_{CE(norm)}$ as a function of the Raman intensity ratio I_C^{RS}. Also indicated are the maximum doping concentrations evaluated from the gas phase doping concentrations PC using a built-in factor and a doping efficiency of one.*

technique measures the number of spins in a particular amount of material. Because the CE resonance only originates from the crystalline phase, one would expect that the density decreases with increasing amorphous content. This can be seen for the low level doped samples, where the spin density N_{CE} decreases by about one order of magnitude with decreasing crystallinity from $I_C^{RS} = 0.47$ to 0.08. Fig. 5.5 (b) shows N_{CE} against the gas phase doping concentration. For the crystalline low defect material ($I_C^{RS} = 0.72 - 0.47$) N_{CE} increases nearly linearly with a structure independent slope as a function of increasing gas phase doping concentration. On the other hand, the influence of the high dangling bond density $N_{DB} = 7.2 \times 10^{16}$ cm^{-3} (for $I_C^{RS} = 0.82$ material) and the low crystalline volume fraction ($I_C^{RS} = 0.08$) results in lower CE intensities. For higher doping concentrations these effects are less pronounced and result in higher CE spin densities.

To account for the fact that the CE signal originates only from the crystalline phase of the μc-Si:H material, the CE spin densities N_{CE} were normalized with respect to the crystalline volume content I_C^{RS}. The results are plotted in Fig. 5.6. Also indicated in Fig. 5.6 are the maximum dopant densities calculated with a built-in factor of one and a doping efficiency of unity, taken with respect to the atomic density of silicon of 5×10^{22} cm^{-3}. For example, $PC = 1$ ppm corresponds to a donor density of 5×10^{16} cm^{-3}. Apparently, with this simple normalization procedure, the influence of the structural change on N_{CE} (Fig. 5.5 (a)) can completely be compensated. Independent of the structure composition, $N_{CE(norm)}$ increases as a function of the doping concentration. On the other hand, $N_{CE(norm)}$ increases with decreasing I_C^{RS}, saturating at the value of the maximum doping

concentration evaluated from the gas phase doping concentration PC. This is in agreement with the decreasing defect density observed in undoped material (compare Fig. 4.5 (a)), proving that the occupation of conduction band-tail states is governed by the compensation of gap states.

5.6 Discussion

In section 4.4 the spin densities N_S of intrinsic microcrystalline material of various structure compositions were discussed. However, as ESR only detects single occupied states D^0 it remains unclear to what extent the measured N_S is related to the real defect density of the material. In this Chapter, ESR in combination with conductivity measurements were applied on n-type μc-Si:H with different phosphorous doping concentrations PC and different structure compositions I_C^{RS} to study the density of gap states and the influence of these states on the free charge carrier density. PC was chosen to be close to the defect density, where the doping induced Fermi level (E_F) shift is determined by the compensation of gap states.

The results confirm that in μc-Si:H, like in a-Si:H, the doping induced Fermi level shift is governed by the compensation of gap states for doping concentrations up to the dangling bond density N_{DB}. Doping induced changes can be observed in both, the ESR signal and the electrical conductivity. While the electrical conductivity increases, in ESR the increasing intensity of the CE resonance indicates a shift of E_F as a function of PC. This confirms the close relation between the dark conductivity σ_D of μc-Si:H at 300K and the spin density of the CE resonance N_{CE}, that have led authors to assign the CE signal to localized states close to the conduction band [30, 29, 36, 72]. However, this is known for a long time. Far more interesting is the fact that both σ_D and N_{CE} are moderated in the same way by the defect density N_{DB}. Doping induced changes are highest for material where low spin densities are found in the undoped state. For highly crystalline material, that also exhibits the highest spin densities, the doping induced changes are considerably less. In other words, the higher DB density observed in highly crystalline material results in lower values of conductivity and lower N_{CE} as a function of the doping concentration. On the other hand, for samples with a low crystalline volume fraction of $I_C^{RS} = 0.08$ the much lower DB density allows much higher σ_D and N_{CE}, the latter normalized to the crystalline volume fraction (Fig. 5.6).

It is surprising, that by doing this normalization the maximum N_{CE} obtained at $I_C^{RS} = 0.08$ is in very good quantitative agreement with the values of the maximum dopant concentration calculated from the gas phase doping concentration, PC.

This suggests a built-in coefficient of phosphorous into the Si-matrix and active donor concentration of unity, if one excludes charge transfer from the amorphous phase. Keeping in mind the characteristic of the spin density N_{DB} of the undoped material, the results are in agreement with the proposed doping mechanism and confirm that the measured N_{DB} represents the defect density in the material. In a simple picture, defects in the gap of μc-Si:H, or more precisely, states in energy below the phosphorus donor states, have to be filled up first before the Fermi level can be shifted into conduction band-tail states, where the majority of the electrons is located which contribute to the CE resonance at 40 K. Tacitly also this assumes, that the phosphorus donor states are located in a position close to the conduction band like in crystalline silicon and that the majority of defects contributing to N_{DB}, no matter where they are located (inside the crystalline cluster columns; at the cluster boundaries; in the disordered regions) affect the E_F shift. It seems important to note, that the observed built-in ratio of P into the Si-matrix of unity somewhat differs from values observed in earlier investigations, where within some scatter a value of about 0.5 has been found [30, 32]. As these authors studied only highly crystalline material, the built-in ratio might vary upon different growth conditions.

From great importance is the energetic distribution of the paramagnetic states within the band gap of the μc-Si:H material. While the intensity of the CE resonance increases with increasing doping concentration, surprisingly the DB resonance is observable in all spectra. From the measurements presented in this chapter it is, however, not possible to distinguish between both DB centers (db_1 and db_2) and therefore only their sum will be discussed here.

The rather strong overlap of more than 0.1 eV suggest that the CE and DB states are spatially separated from each other. This further supports the suggestions made in section 4.4, where the DB resonance, in particular the db_2, was attributed to states located in hydrogen reach regions at the column boundaries. On the other hand, it is a widely accepted fact that the CE signal originates from the crystalline phase of μc-Si:H. Additional support for this thesis comes from Zhou et al., who used electron-spin-echo envelope modulation (ESEEM) to measure the interaction of the unpaired electron with its surrounding nuclear spins [165]. The finding was that the echo decay of the DB signal is modulated by the ^{1}H nuclei, while no modulation of the CE echo decay could be found. This suggests, that the DB centers are located in hydrogen rich regions, whereas the CE centers arise from hydrogen depleted parts of the μc-Si:H films. Although these results could not be confirmed yet, they still support the considerations made in this work.

Why does the spatial separation lead to an energetic overlap of the db_2 and the CE states? Keeping in mind that the column boundaries also represent the interface between the crystalline phase and the disordered material a schematic

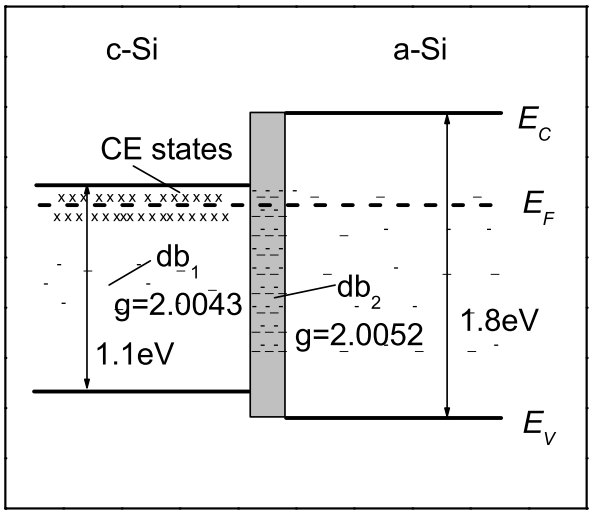

Figure 5.7: *Schematic band diagram of the transition region between the crystalline and disordered phase in μc-Si:H.*

band diagram as shown in Fig. 5.7 can be drawn. The results support an earlier suggestion that in μc-Si:H there should exist a considerable conduction band offset between the crystalline regions (for which the crystalline silicon band gap E_G = 1.1 eV is assumed) and the disordered regions (for which the a-Si:H gap E_G = 1.8 eV is assumed [65]). This would result in a significant overlap between the energy of DB and CE center as shown in Fig. 5.7. Otherwise the simultaneous occurrence of the CE and the DB signal for significant E_F shifts are difficult to explain if one does not allow for strong potential fluctuations in the material. Apparently, this earlier assumption concluded from dark and light induced ESR studies on highly crystalline material is valid even in material with very small crystalline volume fraction [30]. Even for material with $I_C^{RS} = 0.08$ containing only a minute amount of the crystalline phase, i.e., crystalline grains strongly diluted in the amorphous matrix, doping concentration as low as 5×10^{16} cm^{-3} can shift the Fermi level into the conduction band-tail of the crystallites and activate a stable CE resonance.

5.7 Summary

The doping induced Fermi level shift in μc-Si:H, for a wide range of structural compositions, is governed by the compensation of defect states for doping concentrations up to the dangling bond spin density. For higher doping concentrations a doping efficiency close to unity is found. The close relationship between the CE resonance intensity and the conductivity is confirmed, which means the elec-

trons contributing to the CE signal represent the majority of the charge carriers contributing to electric transport. The fact, that for low defect material the N_{CE} approaches the value of the maximum doping concentration, proves the close relation between phosphorus concentration N_P and N_{CE}. However, while in earlier investigations a built-in factor of 0.5 and a doping efficiency of unity was found the results presented here suggest that both are of the order of unity, assuming that charge transfer from the amorphous phase can be excluded. Measuring the real phosphorous concentration using high resolution ion mass spectroscopy (SIMS)[1] could resolve this puzzle and will be a task for future experiments. A significant conduction band off-set between crystalline and disordered regions in μc-Si:H is suggested in agreement with earlier studies.

[1]Note, that the sensitivity limit of a quadrupole mass spectrometer for the measurement of P-concentrations exceeds several 10^{18} cm^{-3}, due to the presence of silicon hydrides of nearly the same mass as the phosphorous ions. Using a high resolution mass spectrometer, the mass defect between ^{31}P and the different silicon hydrides can be used to discriminate between the respective ions.